JACS
JOURNAL OF THE AMERICAN CHEMICAL SOCIETY
Communication
pubs.acs.org/JACS

Enhanced Bifunctional Oxygen Catalysis in Strained $LaNiO_3$ Perovskites

Jonathan R. Petrie,[†] Valentino R. Cooper,[†] John W. Freeland, [§] Tricia L. Meyer,[†] Zhiyong Zhang,[‡] Daniel A. Lutterman,[‡] and Ho Nyung Lee*[,†]

[†]Materials Science and Technology Division and [‡]Chemical Sciences Division, Oak Ridge National Laboratory, Oak Ridge, Tennessee 37831, United States

[§]Advanced Photon Source, Argonne National Laboratory, Argonne, Illinois 60439, United States

Supporting Information

ABSTRACT: Strain is known to greatly influence low-temperature oxygen electrocatalysis on noble metal films, leading to significant enhancements in bifunctional activity essential for fuel cells and metal-air batteries. However, its catalytic impact on transition-metal oxide thin films, such as perovskites, is not widely understood. Here, we epitaxially strain the conducting perovskite $LaNiO_3$ to systematically determine its influence on both the oxygen reduction and oxygen evolution reaction. Uniquely, we found that compressive strain could significantly enhance both reactions, yielding a bifunctional catalyst that surpasses the performance of noble metals such as Pt. We attribute the improved bifunctionality to strain-induced splitting of the e_g orbitals, which can customize orbital asymmetry at the surface. Analogous to strain-induced shifts in the d-band center of noble metals relative to the Fermi level, such splitting can dramatically affect catalytic activity in this perovskite and other potentially more active oxides.

Advancements in energy storage are essential for driving the development of more sophisticated mobile technologies as well as continuing the trend toward a greener economy. At the forefront of this push are high energy density devices, such as regenerative fuel cells and metal-air batteries.[1] In these and related electrochemical systems, both the oxygen reduction and oxygen evolution reactions (ORR and OER, respectively) are crucial toward successful operation.[2] Traditionally, conductive catalysts incorporating noble metals (e.g., Pt and IrO_2) have been used to facilitate these reactions near room temperature.[3] To alleviate costs and poor stabilities during OER in alkaline solutions, significant efforts have focused on transition-metal oxides (TMOs) with multivalent Ni, Fe, Co, and Mn.[4] Similar to alloying in noble metals, the majority of research into increasing oxygen activities of TMOs involves cationic doping, which often promotes either the ORR or OER but not bifunctionality.[5] Here, we explore how another factor, i.e., strain, can influence bifunctionality in TMOs.

Contemporary work on high-temperature (>500 °C) oxide catalysis in an aprotic environment (e.g., ORR: $O_2 + 4e^- \rightarrow 2O^{2-}$) has emphasized the importance of tensile strain for activating defects to improve catalytic reactions.[6] In an alkaline environment (e.g., ORR: $O_2 + 2H_2O + 4e^- \rightarrow 4OH^-$), the reaction pathways are different, and the activities of these defects are reduced. While recent studies have suggested that tensile strain may increase catalysis in some cobaltites, there is no systematic understanding of strain effects in TMOs.[7] On the other hand, these effects are well-characterized for noble metals, where variations in strain can tailor metal−oxygen (M−O) adsorbate/intermediate bond strengths to optimized levels for catalysis, i.e., the Sabatier principle.[8] For instance, an excessive M−O chemisorption in Pt group metals hinders ORR catalysis. Compressive strain shifts the σ^* antibonding states near the Fermi level (E_F) lower in energy, decreasing such chemisorption.[9] Among TMOs, the ABO_3 perovskites, in which A is traditionally from Groups I−III and B is a transition-metal ion with six-fold octahedral coordination, also have electronic structures that are sensitive to strain. Due to strong hybridization between the O 2p and the transition-metal d_{z^2} and $d_{x^2-y^2}$ lobes in the BO_6 octahedra, the σ^* states near E_F consist of e_g orbitals.[10,10b] Similar to the Jahn−Teller distortion, strain is known to lift the degeneracy in these symmetry-localized d_{z^2} and $d_{x^2-y^2}$ orbitals, yielding changes in the orbital occupancy or polarization.[7a,11] By using strain to control the degree of this e_g orbital splitting and polarization in the octahedra, we anticipated that, analogous to noble metals, we could tailor the perovskite oxygen chemisorption and, hence, catalysis.

To examine the effects of strain on the bifunctional activity of perovskites, we used epitaxial $LaNiO_3$ (LNO) films. LNO is a well-known conducting perovskite at room temperature, eliminating the need for a conducting carbon additive that would influence activity.[12] Moreover, LNO in the bulk form is already more catalytic than Pt toward the OER,[7a] though it has not yet shown higher activity than $NiFeO_x$ and α-Mn_2O_3.[4c,13] Similar to the other oxides, its bifunctionality is limited by a lower activity toward the ORR.[14] Since the rate-determining step (RDS) in both reactions is linked to excessive Ni−O chemisorption to hydroxyl groups, tuning these energies through strain could enhance both ORR and OER.[5b,9b,15] Furthermore, the Ni^{3+} (d^7) ion in LNO has a stable low-spin (LS) $t_{2g}^6e_g^1$ configuration.[16] In addition to recent evidence showing that perovskites with an e_g-filling of 1 e^- are promising oxygen electrocatalysts,[14b] the robust LS e_g^1 occupation allows us to focus solely on symmetry changes within the e_g orbitals. Finally,

Received: November 20, 2015
Published: February 11, 2016

DOI: 10.1021/jacs.5b11713
J. Am. Chem. Soc. 2016, 138, 2488−2491

LNO in alkaline solution is stable over a wide range of potentials involving the ORR and OER.[17]

To systematically introduce strain to (001) LNO, epitaxial films (10 nm in thickness) were deposited by pulsed laser epitaxy on a range of lattice-mismatched substrates, which included (001) $LaSrAlO_4$ (LSAO), (001) $LaAlO_3$ (LAO), (001) $(LaAlO_3)_{0.3}(SrAl_{0.5}Ta_{0.5}O_3)_{0.7}$ (LSAT), (001) $SrTiO_3$ (STO), and $(001)_{pc}$ $DyScO_3$ (DSO). As seen by the shift of X-ray diffraction (XRD) peaks in θ–2θ scans, the near-atomically flat surface from AFM, and electrical transport measurements (Figures S3 and S4), these 10 nm thick (001)-oriented films were all of high quality, conductive, and under biaxial strain from 2.7 to −1.2%. Both pre- and post-test XRD and specific area measurements (see SI) were similar, suggesting minimal instability and phase segregation.[13b,18] Using XRD reciprocal space mapping to determine in-plane lattice parameters, we found all films were coherently strained except for LNO on LSAO, which was relaxed and substantially strain free (ε = 0 to −0.3%) due to a small critical thickness for strain relaxation. While an additional range of strain states from ε = −1.2 to 0% was also generated through strain relaxation by increasing the thickness of LNO on LAO from 10 to 100 nm (see Figure S5a), studies on decreasing its thickness on LSAO to minimize strain relaxation are not shown due to systematic limitations measuring films thinner than 5 nm via XRD. As the strain ranged from tensile (+) to compressive (−), the tetragonality or ratio between out-of-plane to in-plane lattice parameters increased from 0.96 to 1.04.

We electrochemically characterized the effects of strain on each film in an oxygen-saturated 0.1 M KOH solution (see SI).[13b] A 50 nm Pt film is used for comparison. As depicted in Figure 1b,c, both the 10 nm films on lattice mismatched substrates as well as the thickness-dependent measurements on LAO (Figure S5b–e) indicate that there is a clear trend toward enhanced catalytic activity with compressive strain for both ORR and OER. Onset potentials clearly shift toward lower overpotentials (η) for both reactions by at least 50 mV between strain states of 2.7 and −1.2%. When current densities (J) for ORR and OER at a typical operating η = 400 mV are compared (Figure 1d), we find that the bifunctional activity drastically increases with compressive strain, showing more than an order of magnitude enhancement. Additionally, the Tafel slopes (Figure S6) are similar to Pt for the LNO films at all strain states, indicating that the RDSs may be similar.[19] To quantify the bifunctional potential, the total η required to reach 30 μA/cm^2 (J_{ORR} at η = 400 mV on the ε = −1.2% LNO) for both ORR and OER is plotted in Figure 1e. Due to decreases in η for both reactions, the highest compressively strained LNO (ε = −1.2%) has a bifunctionality exceeding that of Pt. The difference in total η between compressed LNO and Pt over a wider ORR/OER J range is shown in Figure S7. Furthermore, as seen in Figure S8, both ORR and OER enhancements do not simply correlate with strain-induced changes in electrical conductivity, precipitating a more in-depth examination of the electronic structure.

As shown in Figure 2, we used X-ray absorption spectroscopy (XAS) on the Ni-L_2 edge to characterize the electronic basis behind the strain-induced modulation in activity.[11b,20] There is no shift in the polarization-averaged edge, indicating stoichiometric Ni^{3+} with an insignificant amount of oxygen defects in our LNO films (Figure S9). The shoulder features on the leading edges are a consequence of localized carriers in more insulating charge-ordered LNO.[11b] To resolve the orbital splitting energies and e_g^1 occupancies between the d_{z^2} and $d_{x^2-y^2}$ orbitals, we

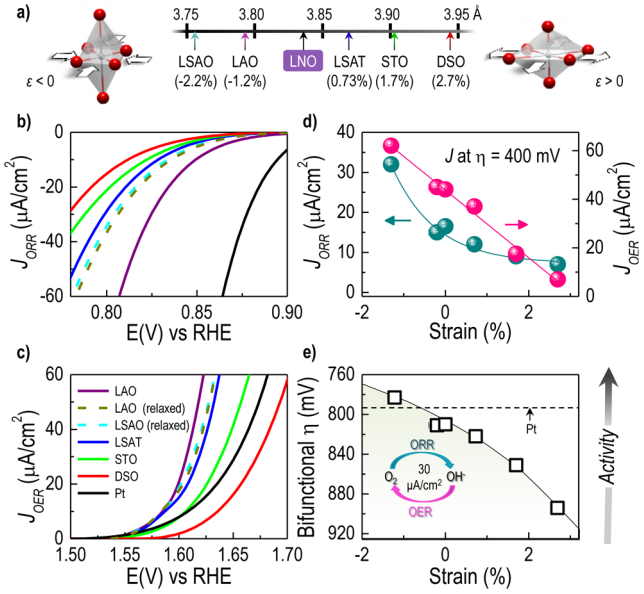

Figure 1. Enhanced ORR and OER bifunctional activities using compressive strain. (a) Lattice parameters and associated biaxial strain for LNO on various substrates. Polarization curves for the (b) ORR and (c) OER on these strained LNO films. Strain-relaxed ($\varepsilon \sim 0\%$) films grown on LSAO (10 nm in film thickness) and on LAO (100 nm in film thickness) as well as Pt films are used for comparison. (d) Current densities (J) of both reactions at overpotentials of η = 400 mV (ORR = 0.823 V and OER = 1.623 V) increase with compressive strain. (e) Bifunctional η to attain 30 μA/cm^2 for both reactions show compressed $LaNiO_3$ surpassing Pt and IrO_2.

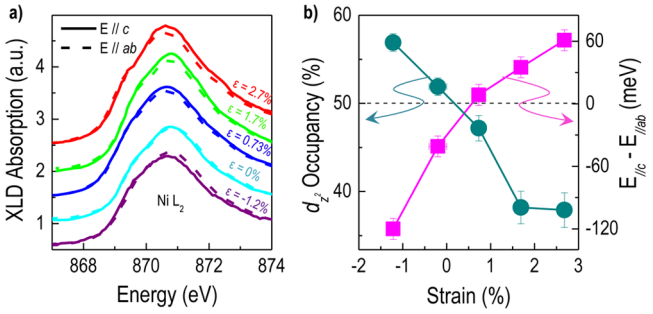

Figure 2. XLD characterization of orbital splitting and polarization. (a) XLD spectra (FY) of the Ni L_2 edge for the strained LNO films. Absorption along the c-axis (ab-axis) corresponds to holes in the d_{z^2} ($d_{x^2-y^2}$) orbital. (b) Using sum rules, strain-induced changes in the occupancy of the d_{z^2} orbital along with the relative energy positions of the d_{z^2} orbital compared to the $d_{x^2-y^2}$ orbital ($E_c - E_{ab}$) are plotted.

employed X-ray linear dichroism (XLD). As seen in Figure 2a, by detecting the absorption of X-rays polarized both perpendicular (E // c) and parallel to the film plane (E // ab), we were able to probe the respective energies and unoccupied states (holes) of the d_{z^2} and $d_{x^2-y^2}$ orbitals.[10b,21] Comparing the difference in the peak energy values between the c- and ab-axes edges, we notice that compressive strain reduces the peak energy of the d_{z^2} orbital compared to the $d_{x^2-y^2}$ orbital, while tensile strain has the opposite effect. Furthermore, the d_{z^2} orbital occupancy can be quantitatively determined through sum rules and assumptions originally developed to examine strained LNO heterostructures (see SI).[21,22] By plotting this peak position and orbital occupancy as a function of strain in Figure 2b, we can see that compressive (tensile) strain-induced orbital splitting results in a lower-energy,

DOI: 10.1021/jacs.5b11713
J. Am. Chem. Soc. 2016, 138, 2488–2491

high-occupancy d_{z^2} ($d_{x^2-y^2}$) orbital. Although the XLD data shown are from fluorescence yield (FY), the result from total electron yield (TEY) is similar. Note that in both cases, the penetration depth is at least 5−10 nm, which involves probing the entire film.

To further investigate the electronic effects at the extreme surface, we computationally modeled the LNO structure using density functional theory (DFT) calculations in vacuum for strain states from −3 to 3% (see SI). The results are shown in Figures S10 and S11 for both the bulk (5 monolayers) and the surface (top layer). Orbital splitting was determined by calculating the centroid of all states for each orbital relative to E_F, excluding the strongly hybridized Ni 3d - O 2p states below approximately −4 to −3 eV, (analogous to the d-band center in metals), and the orbital polarization was found by calculating the orbital e^- occupancy. As seen in Figure 3a, calculations for the

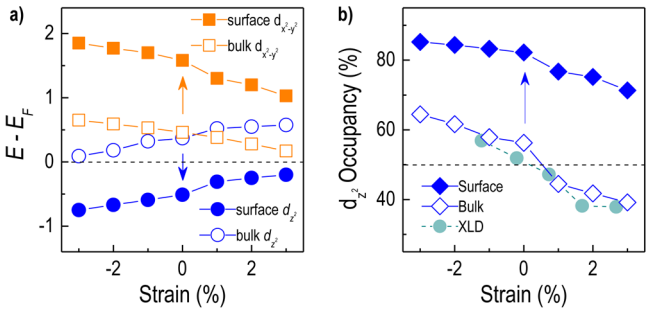

Figure 3. Computational modeling of orbital splitting and polarization. (a) Strain-dependent changes in the centroid position of density of states (DOS) for the d_{z^2} and $d_{x^2-y^2}$ orbitals with respect to E_F for both the LNO bulk and surface. Arrows are used to guide the eye from bulk to surface data. (b) Modeled orbital polarization in the bulk closely follows the experimental XLD data (shown from Figure 2b), while the asymmetric surface occupancy is biased toward d_{z^2}.

bulk match the experimental XLD results where compressive (tensile) strain favors a more polarized d_{z^2} ($d_{x^2-y^2}$) orbital of lower energy. However, the surface calculations reveal a much different result due to the asymmetry resulting from the lack of an apical oxygen atom on the surface NiO_6 octahedra. While the total e^- occupancy of the e_g states is ∼1 in all cases, this asymmetry leads to a ∼1 eV decrease (increase) in the center of the d_{z^2} ($d_{x^2-y^2}$) orbital relative to E_F. Even though strain-induced orbital splitting still occurs at the surface, these offsets result in the d_{z^2} ($d_{x^2-y^2}$) orbital center lying below (above) E_F over the entire strain range. Correspondingly, as shown in Figure 3b, the orbital polarization at the surface is shifted toward the d_{z^2} orbital; indeed, the occupancy of this orbital in unstrained LNO increases from ∼55% of e_g^1 in the bulk to ∼80% at the surface. Thus, the asymmetry at the surface dramatically favors occupancy of the d_{z^2} orbital over the $d_{x^2-y^2}$ orbital. Similar trends favoring the d_{z^2} orbital occur when the apical position during the RDS is occupied by an adsorbate that is a weaker field ligand on the spectrochemical series, i.e., trending toward vacuum, than the O^{2-} anions in the perovskite BO_6 octahedral structure. Here, the hydroxyl ions are indeed weaker field ligands than O^{2-}, resulting in a similar asymmetric surface.[23]

Interestingly, the trend we detected between strain and oxygen activity in a perovskite such as LNO is comparable to that seen in the Pt group metals. In both cases, a compressive strain-induced weakening of the M−O chemisorption enhances the activity. As seen in Figure 4b for Pt, variations in bandwidth due to strain

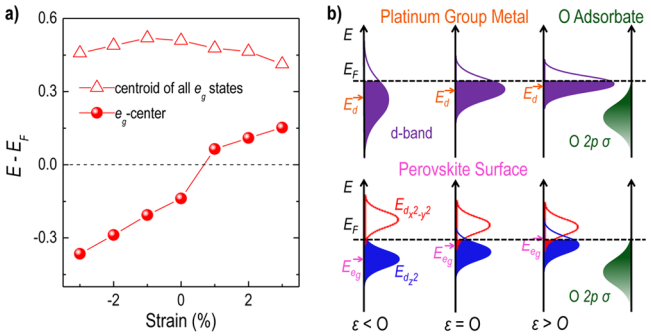

Figure 4. The e_g center rationalization of the DFT results for strain-induced changes in electrocatalytic activity. (a) Position of the centroids calculated from DOS for the e_g states and the e_g-center (E_{e_g}) with respect to E_F as a function of strain. E_{e_g} decreases (increases) with compressive (tensile) strain. (b) Schematics relating this trend in perovskites to the d-band center (E_d) in Pt. While changes in bandwidth play a significant role in E_d shifts for Pt group metals, orbital splitting and polarization have a greater effect at the asymmetric surface of correlated oxides such as LNO.

within a uniformly filled d-band can shift its center (E_d) with respect to E_F. Compressive strain broadens the band, essentially lowering E_d to increase σ^* occupancy and destabilize the M−O bond. For the small shifts in E_d associated with strain, there is a linear relationship between changes in E_d and M−O chemisorption energy.[23] Extrapolating this concept to LNO, we plotted the combined center of both e_g orbitals ($d_{z^2} + d_{x^2-y^2}$) as a function of strain in Figure 4a and found no similar monotonic shift that would explain weakening of the M−O bond and subsequent increase in oxygen activity. However, unlike the d-band theory for metals, the e_g orbitals at the surface of a correlated oxide become localized, implying, as seen by the DFT results, that (1) strain broadening can be less significant than strain-induced shifts in orbital energies and (2) the e_g orbital with greater e^- occupancy will have a larger influence on M−O chemisorption. Consequently, instead of simply totaling orbital states, we weighted the center of each state to its orbital occupancy at the surface to determine the e_g-center (E_{e_g}). Due to the disparity of polarization toward the d_{z^2} orbital, its influence in the M−O strength is disproportionate to that of $d_{x^2-y^2}$, which is consistent with a geometric argument postulating greater overlap between O 2p adsorbate orbitals and the d_{z^2} states at the solution interface. As shown in Figure 4, E_{e_g} trends toward lower energies with compressive strain, which results in weaker M−O chemisorption and a subsequent enhancement in the catalytic activity. Therefore, by examining both the orbital splitting and polarization at the surface of LNO, we suggest a new parameter, E_{e_g}, to predict strain-induced changes in ORR and OER activities in this perovskite and related oxides.

In summary, by investigating the hitherto unexplored effects of strain on the oxygen electrocatalytic activity of LNO perovskite films, we have shown that compressive strain as small as −1.2% can enhance the bifunctional ORR and OER activities above that of the best performing noble metal. While the catalytic trends are akin to strain-induced bandwidth changes in the d-band center of noble metals, we have described an e_g-center that depends on both orbital splitting and polarization effects at the asymmetric surface to describe shifts in activity. Although applied to a perovskite, there is no reason such strain cannot increase the activity of other TMO-based catalysts, such as Mn_2O_3 and

DOI: 10.1021/jacs.5b11713
J. Am. Chem. Soc. 2016, 138, 2488−2491

$NiFeO_x$. Previously, the possibilities of tensile strain on LNO-based heterostructures have attracted great interest due to physical properties, such as theoretical hints of cuprate-like superconductivity.[24] Here, our new discovery further expands the importance of strain engineering TMOs into the electrochemical realm.

■ ASSOCIATED CONTENT

Supporting Information

The Supporting Information is available free of charge on the ACS Publications website at DOI: 10.1021/jacs.5b11713.

Experimental details and data (PDF)

■ AUTHOR INFORMATION

Corresponding Author

*hnlee@ornl.gov

Notes

The authors declare no competing financial interest.

■ ACKNOWLEDGMENTS

We acknowledge S. Okamoto for theoretical insight. This work was supported by the U.S. Department of Energy (DOE), Office of Science (OS), Basic Energy Sciences (BES), Materials Science and Engineering Division (synthesis, physical property characterization, and XAS data analysis) and by the Laboratory Directed Research and Development Program of Oak Ridge National Laboratory, managed by UT-Battelle, LLC, for the U.S. DOE (electrochemical characterization and theory). Reference electrode preparation was performed as a user project at the Center for Nanophase Materials Sciences, which is sponsored at Oak Ridge National Laboratory by the Scientific User Facilities Division, BES, U.S. DOE. Use of electrochemical testing system was supported by the Fluid Interface Reactions, Structures, and Transport (FIRST) Center, an Energy Frontier Research Center funded by the U.S. DOE, OS, BES. Use of the Advanced Photon Source for XAS was supported by the U.S. DOE, OS, under contract no. DE-AC02-06CH11357.

■ REFERENCES

(1) (a) Winter, M.; Brodd, R. J. *Chem. Rev.* **2004**, *104*, 4245. (b) Watanabe, M.; Tryk, D. A.; Wakisaka, M.; Yano, H.; Uchida, H. *Electrochim. Acta* **2012**, *84*, 187.

(2) (a) Fabbri, E.; Habereder, A.; Waltar, K.; Kotz, R.; Schmidt, T. J. *Catal. Sci. Technol.* **2014**, *4*, 3800. (b) Debe, M. K. *Nature* **2012**, *486*, 43.

(3) Gasteiger, H. A.; Kocha, S. S.; Sompalli, B.; Wagner, F. T. *Appl. Catal., B* **2005**, *56*, 9.

(4) (a) Nie, Y.; Li, L.; Wei, Z. *Chem. Soc. Rev.* **2015**, *44*, 2168. (b) Bockris, J. O.; Otagawa, T. *J. Phys. Chem.* **1983**, *87*, 2960. (c) Gorlin, Y.; Jaramillo, T. F. *J. Am. Chem. Soc.* **2010**, *132*, 13612. (d) Akhade, S. A.; Kitchin, J. R. *J. Chem. Phys.* **2012**, *137*, 084703.

(5) (a) Suntivich, J.; Gasteiger, H. A.; Yabuuchi, N.; Nakanishi, H.; Goodenough, J. B.; Shao-Horn, Y. *Nat. Chem.* **2011**, *3*, 546. (b) Yildiz, B. *MRS Bull.* **2014**, *39*, 147. (c) Młynarek, G.; Paszkiewicz, M.; Radniecka, A. *J. Appl. Electrochem.* **1984**, *14*, 145. (d) Singh, R. N.; Singh, J. P.; Lal, B.; Thomas, M. J. K.; Bera, S. *Electrochim. Acta* **2006**, *51*, 5515.

(6) Stoerzinger, K. A.; Choi, W. S.; Jeen, H.; Lee, H. N.; Shao-Horn, Y. *J. Phys. Chem. Lett.* **2015**, *6*, 487.

(7) (a) Bockris, J. O. M.; Otagawa, T. *J. Electrochem. Soc.* **1984**, *131*, 290. (b) Norskov, J. K.; Bligaard, T.; Rossmeisl, J.; Christensen, C. H. *Nat. Chem.* **2009**, *1*, 37.

(8) Stamenkovic, V. R.; Fowler, B.; Mun, B. S.; Wang, G.; Ross, P. N.; Lucas, C. A.; Marković, N. M. *Science* **2007**, *315*, 493.

(9) (a) Marković, N. M.; Schmidt, T. J.; Stamenković, V.; Ross, P. N. *Fuel Cells* **2001**, *1*, 105. (b) Greeley, J.; Stephens, I. E. L.; Bondarenko, A. S.; Johansson, T. P.; Hansen, H. A.; Jaramillo, T. F.; Rossmeisl, J.; Chorkendorff, I.; NÃrskov, J. K. *Nat. Chem.* **2009**, *1*, 552. (c) Stamenkovic, V. R.; Mun, B. S.; Arenz, M.; Mayrhofer, K. J. J.; Lucas, C. A.; Wang, G.; Ross, P. N.; Markovic, N. M. *Nat. Mater.* **2007**, *6*, 241. (d) Hong, W. T.; Risch, M.; Stoerzinger, K. A.; Grimaud, A.; Suntivich, J.; Shao-Horn, Y. *Energy Environ. Sci.* **2015**, *8*, 1404.

(10) (a) Grimaud, A.; May, K. J.; Carlton, C. E.; Lee, Y.-L.; Risch, M.; Hong, W. T.; Zhou, J.; Shao-Horn, Y. *Nat. Commun.* **2013**, *4*, 3439. (b) Pesquera, D.; Herranz, G.; Barla, A.; Pellegrin, E.; Bondino, F.; Magnano, E.; Sánchez, F.; Fontcuberta, J. *Nat. Commun.* **2012**, *3*, 1189.

(11) (a) Freeland, J. W.; Jian, L.; Kareev, M.; Gray, B.; Kim, J. W.; Ryan, P.; Pentcheva, R.; Chakhalian, J. *Europhys. Lett.* **2011**, *96*, 57004. (b) Tung, I. C.; Balachandran, P. V.; Liu, J.; Gray, B. A.; Karapetrova, E. A.; Lee, J. H.; Chakhalian, J.; Bedzyk, M. J.; Rondinelli, J. M.; Freeland, J. W. *Phys. Rev. B: Condens. Matter Mater. Phys.* **2013**, *88*, 205112.

(12) Otagawa, T.; Bockris, J. O. M. *J. Electrochem. Soc.* **1982**, *129*, 2391.

(13) (a) Merrill, M. D.; Dougherty, R. C. *J. Phys. Chem. C* **2008**, *112*, 3655. (b) McCrory, C. C. L.; Jung, S.; Peters, J. C.; Jaramillo, T. F. *J. Am. Chem. Soc.* **2013**, *135*, 16977.

(14) (a) Hardin, W. G.; Mefford, J. T.; Slanac, D. A.; Patel, B. B.; Wang, X.; Dai, S.; Zhao, X.; Ruoff, R. S.; Johnston, K. P.; Stevenson, K. J. *Chem. Mater.* **2014**, *26*, 3368. (b) Suntivich, J.; May, K. J.; Gasteiger, H. A.; Goodenough, J. B.; Shao-Horn, Y. *Science* **2011**, *334*, 1383.

(15) Medarde, M. L. *J. Phys.: Condens. Matter* **1997**, *9*, 1679.

(16) Volodin, A. A.; Fursikov, P. V.; Belmesov, A. A.; Shulga, Y. M.; Khodos, I. I.; Abdusalyamova, M. N.; Tarasov, B. P. *Inorg. Mater.* **2014**, *50*, 673.

(17) Chakhalian, J.; Rondinelli, J. M.; Liu, J.; Gray, B. A.; Kareev, M.; Moon, E. J.; Prasai, N.; Cohn, J. L.; Varela, M.; Tung, I. C.; Bedzyk, M. J.; Altendorf, S. G.; Strigari, F.; Dabrowski, B.; Tjeng, L. H.; Ryan, P. J.; Freeland, J. W. *Phys. Rev. Lett.* **2011**, *107*, 116805.

(18) Sakthivel, M.; Bhandari, S.; Drillet, J.-F. *ECS Electrochem. Lett.* **2015**, *4*, A56.

(19) Damjanovic, A.; Dey, A.; Bockris, J. O. M. *J. Electrochem. Soc.* **1966**, *113*, 739.

(20) Benckiser, E.; Haverkort, M. W.; Brück, S.; Goering, E.; Macke, S.; Frañó, A.; Yang, X.; Andersen, O. K.; Cristiani, G.; Habermeier, H.-U.; Boris, A. V.; Zegkinoglou, I.; Wochner, P.; Kim, H.-J.; Hinkov, V.; Keimer, B. *Nat. Mater.* **2011**, *10*, 189.

(21) Wu, M.; Benckiser, E.; Haverkort, M. W.; Frano, A.; Lu, Y.; Nwankwo, U.; Brück, S.; Audehm, P.; Goering, E.; Macke, S.; Hinkov, V.; Wochner, P.; Christiani, G.; Heinze, S.; Logvenov, G.; Habermeier, H. U.; Keimer, B. *Phys. Rev. B: Condens. Matter Mater. Phys.* **2013**, *88*, 125124.

(22) Hammer, B.; Nórskov, J. K. *Surf. Sci.* **1995**, *343*, 211.

(23) Hammer, B.; Nielsen, O. H.; Nórskov, J. K. *Catal. Lett.* **1997**, *46*, 31.

(24) Chaloupka, J.; Khaliullin, G. *Phys. Rev. Lett.* **2008**, *100*, 016404.

DOI: 10.1021/jacs.5b11713
J. Am. Chem. Soc. 2016, 138, 2488−2491